

Cascade of phase transitions in the vicinity of a quantum critical point

H. Meier^{1,2}, C. Pépin³, M. Eimenkel², and K. B. Efetov^{2,3,◇}

¹*Department of Physics, Yale University, New Haven, Connecticut 06520, USA*

²*Institut für Theoretische Physik III, Ruhr-Universität Bochum, 44780 Bochum, Germany*

³*IPhT, CEA-Saclay, L'Orme des Merisiers, 91191 Gif-sur-Yvette, France*

◇ *Corresponding author, E-mail : efetov@tp3.rub.de.*

(Dated: August 14, 2018)

We study the timely issue of charge order checkerboard patterns observed in a variety of cuprate superconductors. We suggest a minimal model in which strong quantum fluctuations in the vicinity of a single antiferromagnetic quantum critical point generate the complexity seen in the phase diagram of cuprates superconductors and, in particular, the evidenced charge order. The Fermi surface is found to fractionalize into hotspots and antinodal regions, where physically different gaps are formed. In the phase diagram, this is reflected by three transition temperatures for the formation of pseudogap, charge density wave, and superconductivity (or quadrupole density wave if a sufficiently strong magnetic field is applied). The charge density wave is characterized by modulations along the bonds of the CuO lattice with wave vectors connecting points of the Fermi surface in the antinodal regions. These features, previously observed experimentally, are so far unique to the quantum critical point in two spatial dimensions and shed a new light on the interplay between strongly fluctuating critical modes and conduction electrons in high-temperature superconductors.

I. INTRODUCTION

High-temperature (high- T_c) cuprate superconductors¹⁻³ rank among the most complex materials ever discovered. Despite the rich diversity within the cuprate family, all compounds share common features such as the antiferromagnetic Mott insulator phase at zero or small doping. Magnetic fluctuations are ubiquitously present in all compounds of the cuprate family. Upon hole-doping of the copper-oxide planes, they become superconductors at unusually high transition temperatures T_c . Ultimately, at intermediate doping, they exhibit the enigmatic pseudo-gap phase characterized by a gap observed in transport and thermodynamics up to a temperature $T^* > T_c$.

In the last years, incommensurate charge modulations have been reported in many of the families' compounds. These modulations form a checkerboard pattern and possibly also break nematicity.⁴⁻¹² Complimentary to each other, these experiments demonstrate that this order is different from stripe spin-charge modulations predicted earlier^{13,14}, observed in La-compounds¹⁵, and discussed in numerous publications (see, e.g., Refs. 16 and 17), as well as from the d -wave order proposed in Ref. 18.

Among the simplest properties common to all the cuprate compounds is the presence of strong antiferromagnetic fluctuations due to the proximity of a doping-driven quantum phase transition between an antiferromagnetic and normal metal phase. Approaching the complexity of the cuprates from the perspective of this *universal* singularity, we provide an extensive study of a single antiferromagnetic two-dimensional quantum critical point (QCP). Proximity to quantum phase transitions^{19,20} is generally believed important to explain the intriguing behavior of high- T_c cuprates^{2,3,21}, heavy fermions²², or doped ferromagnets²³.

Our study unveils that this QCP triggers a cascade of

phase transitions with symmetries different from those of the parent transition. These phases include d -wave superconductivity, a checkerboard structure of quadrupole density wave (QDW), a charge density wave (CDW) with another checkerboard structure turned by 45° with respect to the former, and the “pseudogap state” which lacks any long range order. The additional charge order (CDW) arises due to interaction of electrons with superconducting fluctuations in situations when superconductivity itself is destroyed. To the best of our knowledge, formation of CDW due to superconducting fluctuations has not been considered previously. The complexity of the phase diagram is recovered out of a single original QCP using a low energy effective theory describing interaction between low energy fermions and paramagnons, which represent the quantum fluctuations of the antiferromagnetic order parameter. This unexpected result enriches the conventional picture^{19,20} of a single QCP and may provide new insights into the pseudogap phase of hole-doped cuprates.

II. PHYSICAL PICTURE

Before delving into details of the microscopic derivation, let us first develop the physical picture and phenomenology. In Sec. III we provide a microscopic study to back up the physical picture, and finally, in Sec. IV we address the question how our results may help to understand physical phenomena observed in the high- T_c cuprates.

A. Spin-fermion model and pseudogap state

We adopt the two-dimensional spin-fermion model²⁴ for the antiferromagnetic QCP as the “minimal model”

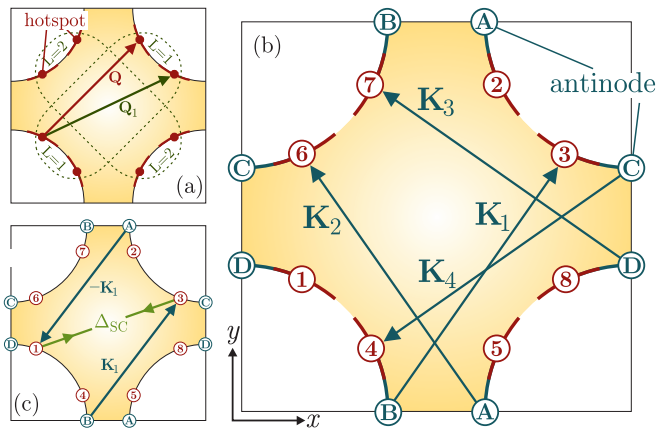


FIG. 1. (a) Brillouin zone and Fermi surface. Quantum critical paramagnons single out eight hotspots that we organize in two quartets ($L = 1$ and $L = 2$). (b) Extended model of hotspot (red) and antinodal states (blue). Non-singular paramagnons with wave vectors $\mathbf{K}_1, \dots, \mathbf{K}_4$ mediate the interaction between hotspot and antinodal states. (c) Cooper pair generation at antinodes **A** and **B**.

in which we seek to understand the diversity of the non-magnetic phases. As has been known for a while^{24,25}, this model features a superconducting instability of the normal metal state. More recently, linearizing the quasiparticle spectrum near so-called “hotspots”, Metlitski and Sachdev pointed out²⁶ an $SU(2)$ particle-hole symmetry of the effective Lagrangian that might lead to another instability toward a “bond order” state. About two years later, it has been noticed²⁷ that, in fact, a state with a complex order parameter comprising both superconductivity and an unusual charge order forms below a certain T^* . These phenomena significantly expand the earlier effective picture²⁸ of free but Landau-damped paramagnons.

In the model considered, spin- $\frac{1}{2}$ fermion quasiparticles $\psi = (\psi_\uparrow, \psi_\downarrow)$, which occupy states close to the Fermi surface shown in Fig. 1(a), couple to paramagnons $\phi = (\phi^x, \phi^y, \phi^z)$ with propagator

$$\langle \phi_{\omega, \mathbf{q}}^\alpha \phi_{-\omega, -\mathbf{q}}^\beta \rangle = \frac{\delta_{\alpha\beta}}{c^{-2}\omega^2 + (\mathbf{q} - \mathbf{Q})^2 + \xi_{AF}^{-2}}, \quad (1)$$

where c is the velocity of paramagnon excitations. At the QCP, the length ξ_{AF} diverges so that the paramagnon propagator becomes singular at the antiferromagnetic ordering wave vector $\mathbf{Q} = (\pm\pi/a, \pm\pi/a)$, where a is the lattice constant of the Cu layer. Quasiparticles emitting or absorbing such singular paramagnons exist only in the vicinity of eight hotspots, see Fig. 1. In a first approximation, we thus focus on these hotspots.

The energy scale $\Gamma \sim \lambda^2$, where λ is fermion-paramagnon coupling constant, determines a temperature $T^* \sim 0.1\Gamma$, below which a complex order with competing charge and d -wave superconducting suborders shows up²⁷ and completely changes major properties of the system. The order parameter in this regime can be

represented in the form $b_0 u$, where $b_0 \sim \Gamma$ is an amplitude and u an unitary matrix in particle-hole space,

$$u = \begin{pmatrix} \Delta_{QDW} & \Delta_{SC} \\ -\Delta_{SC}^* & \Delta_{QDW}^* \end{pmatrix}. \quad (2)$$

In this matrix, Δ_{QDW} and Δ_{SC} are complex amplitudes for charge order and superconductivity, respectively. Unitarity imposes $|\Delta_{QDW}|^2 + |\Delta_{SC}|^2 = 1$. In fact, there are two independent order parameters of the form of Eq. (2), one for each of the two quartets of hotspots, Fig. 1(a), which in the “hotspot-only” approximation are effectively decoupled.

The charge order competing with superconductivity is characterized by a quadrupole moment spatially modulated with wave vectors \mathbf{Q}_1 and \mathbf{Q}_2 , see Fig. 2. These wave vectors connect hotspots opposite to each other with respect to the center of the Brillouin zone but are equivalently represented as in the inset of Fig. 2. The resulting checkerboard structure of this *quadrupole-density wave* (QDW) is shown in Fig. 2(a). The QDW (or, equivalently, “bond order”) instability for wave vectors $\mathbf{Q}_{1,2}$ has been recently confirmed in an unrestricted Hartree-Fock study.²⁹

The matrix order parameter u , Eq. (2), obtained from mean-field equations at temperatures $T < T^*$ is highly degenerate.²⁷ At low enough temperatures, this degeneracy is lifted by curvature and magnetic field effects, the former favoring superconductivity, the latter QDW.³⁰ At high enough temperatures (but still below T^*) thermal fluctuations restore the degeneracy and thus establish a *pseudogap phase* without a specific long-range order. The effective $O(4)$ non-linear σ -model for fluctuations of u (derived in Ref. 27) as well as a more recent $O(6)$ -model³¹ show in many aspects a good agreement with experiments.

B. Antinodal states

The nontrivial order parameter (2) has been derived taking into account only interactions mediated by the critical modes with momenta $\sim \mathbf{Q}$ corresponding to the strongest antiferromagnetic fluctuations. Fermi surface regions beyond the hotspots have not yet been touched by the theoretical treatment and remained gapless in the “hotspot-only” approximation.

For the superconducting suborder, however, it is clear that the gap should cover the entire Fermi surface³², with the exception of the nodes of the d -wave gap function that are situated at the intercept points of the Fermi surface and the diagonals of the Brillouin zone. In particular, we expect a significant superconducting gap also at the so-called *antinodes* situated at the zone edges, see Fig. 1(b). The main result of the present study is that superconductivity is not the only possible order close to the antinodes, and we are going to show that another charge order (CDW) can appear in this region and challenge superconductivity there. Favorably for CDW, opposite

antinodes are effectively nested for a singular interaction. Flatness of the antinodal Fermi surface is not requisite but may enhance this effect.

To be specific, we extend the study of the spin-fermion model by considering both hotspots and antinodes, see Fig. 1(b). In the leading approximation, fermion quasiparticles located close to the antinodes interact with hotspot fermions by exchanging non-singular paramagnons with propagator $\langle \phi^j \phi^j \rangle \simeq [(\Delta K)^2 + \xi_{\text{AF}}^{-2}]^{-1}$ where $\Delta K = |\mathbf{K}_1 - \mathbf{Q}|$ is the distance between hotspots and nearest antinodes, cf. Fig. 1. This interaction is clearly weaker than the interaction between hotspots connected by \mathbf{Q} . On the other hand, it allows quantum criticality to spread into the so far untouched antinodal regions. The smallness of the non-singular propagators justifies a perturbative treatment, whereas singular paramagnons have to be fully accounted for.

We now discuss the effects due to the paramagnon-mediated interaction between hotspot and antinodal quasiparticles. We begin with the case of established superconductivity at the hotspots and then, more interestingly, for the case of hotspots gapped by QDW or pseudogapped hotspots.

Below T_c , hotspot fermions form Cooper pairs. In this case, we may neglect fluctuations and replace pairs of hotspot fermion fields by their mean-field average $\Delta_{\text{SC}} \sim b_0 \langle \psi_{\uparrow,1}^\dagger \psi_{\downarrow,3}^\dagger \rangle$. Let us consider two antinodal quasiparticles situated, e.g., at antinodes **A** and **B**, see Fig. 1(c). Virtually exchanging a paramagnon with wave vector \mathbf{K}_1 , they are scattered to hotspots **1** and **3**. There, they are affected by the established superconducting order Δ_{SC} and thus form Cooper pairs themselves. Interestingly, a similar virtual process is impossible for the particle-hole suborder (QDW) since in this case both particle and hole would have to emit a paramagnon of the same wave vector.

As a result, the explicit mean-field analysis, cf. Eq. (26), yields a superconducting gap at the antinodes, which by a factor of

$$\alpha \sim \frac{\Gamma^2}{v^2 [(\Delta K)^2 + \xi_{\text{AF}}^{-2}]} \quad (3)$$

is smaller than the hotspot gap. Notably, cf. again Eq. (26), the antinodal gap has d -wave symmetry. Moreover, by continuity the antinodal superconductivity fixes the relative phase of the so far decoupled superconducting suborders of the two hotspot quartets in Fig. 1(a), ensuring overall d -wave symmetry of the superconducting order parameter. We note that this mean-field result actually does not require separating the Fermi surface into hotspots and antinodal regions and has been obtained with full momentum resolution.³²

C. Charge density wave

When hotspot superconductivity is destroyed by either thermal fluctuations or a strong magnetic field, the

superconducting gap at the hotspots has zero mean, $\langle \Delta_{\text{SC}} \rangle = 0$, implying absence of antinodal superconductivity as well. However, antinodal quasiparticles still couple to non-zero superconducting fluctuations $\Delta_{\text{SC}}(\mathbf{r}, \tau)$ induced at the antinodes by the same mechanism that produced the antinodal superconducting gap in the preceding section.

In this situation, the superconducting fluctuations mediate an effective interaction between antinodal fermions. Close to the transition, the mass ξ_{SC}^{-2} of superconducting fluctuations is small and the effective interaction becomes critical. This also leads to effective nesting of opposite antinodes. As a result, this situation is remarkably similar to the initial situation of hotspot fermions interacting via critical paramagnons. While quantum-critical paramagnons reorganize the ground state of hotspot quasiparticles into the pseudogap state, the critical superconducting fluctuations play a very similar role at the antinodes and trigger in analogy a transition to another phase. This repeated triggering of orders thus constitutes a *cascade* of phase transitions.

The order parameter formed at the antinodes is pure particle-hole pairing. It cannot be a form of superconductivity because it has to be “orthogonal” to the superconducting fluctuations that mediate the effective interaction. Furthermore, particle-hole pairing at antinodes **A** and **B**, see Fig. 1(b), is independent from particle-hole pairing at **C** and **D**. This can be seen as, e.g., wave vectors \mathbf{K}_1 and \mathbf{K}_2 mediate interactions at antinodes **A** and **B** but have no meaning for **C** and **D**, where involved paramagnons carry wave vectors \mathbf{K}_3 and \mathbf{K}_4 . Invariance under rotations of 90° then inevitably leads to a bidirectional *charge density wave* (CDW) order at the antinodes.

The explicit analysis (see Sec. III) follows the same steps as the mean-field scheme of Ref. 27 for the pseudogap state. This leads us to a similar universal mean-field equation, see Eq. (35), with all relevant energies measured in units of the energy

$$\Gamma_{\text{CDW}} \sim \alpha^2 \Gamma \quad (4)$$

with $\alpha \ll 1$ defined in Eq. (3). A non-zero CDW gap exists at temperatures $T < T_{\text{CDW}} \sim 0.1 \Gamma_{\text{CDW}}$. In realistic cuprate systems, we may expect $T_c < T_{\text{CDW}} < T^*$ as well as comparable energy scales, $\Gamma_{\text{CDW}} \sim \Gamma$. The calculation of charge density $\rho(\mathbf{r})$ in the CDW phase leads to a spatial modulation of the form

$$\rho_{\text{CDW}}(\mathbf{r}) \sim \frac{e \Gamma_{\text{CDW}}^2}{v^2} \{ \cos(\mathbf{Q}_x \mathbf{r} + \varphi_x) + \cos(\mathbf{Q}_y \mathbf{r} + \varphi_y) \}. \quad (5)$$

The wave vectors \mathbf{Q}_x and \mathbf{Q}_y (see Fig. 2) connect opposite antinodes and correspond to a *modulation along the bonds* of the Cu lattice. The resulting pattern is a checkerboard as shown in Fig. 2(b), similarly to the pattern of QDW shown in Fig. 2(a). Notably, the CDW and QDW patterns are turned by 45° with respect to each

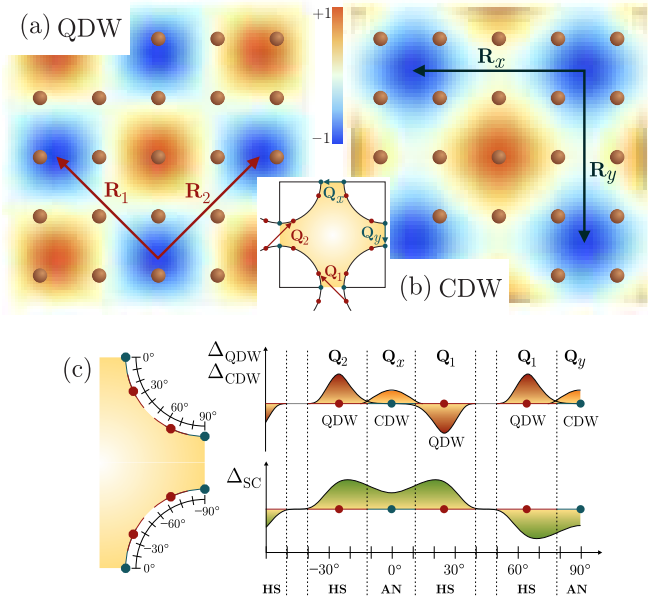


FIG. 2. Checkerboard charge order for the pseudogap sub-order of (a) QDW and (b) antinodal CDW. Modulation vectors \mathbf{Q}_i giving the periods $\mathbf{R}_i = 2\pi\mathbf{Q}_i/|\mathbf{Q}_i|^2$ are shown in the inset. (c) Qualitative dependence of the superconducting and charge order gaps on the position on the Fermi surface (HS = hotspots, AN = antinodes).

other. Variables $\varphi_{x,y}$ denote offset phases. Figure 2(c) summarizes the results of our study by providing a sketch of the emergent orders as a function of the position on the Fermi surface.

III. MICROSCOPIC ANALYSIS

A. Effective Lagrangian

We begin our microscopic analysis by developing a convenient and compact notation for the subsequent calculations. We are mainly interested in the low-lying excitations close to the hotspots and antinodes, which we numerate according to Fig. 1(b) with numbers $j = 1, \dots, 8$ and capital letters $J = A, \dots, D$, respectively. In this spirit, we represent a general quasiparticle field $\psi(\mathbf{r})$ as

$$\psi(\mathbf{r}) = \sum_{j=1}^8 e^{i\mathbf{p}_j\mathbf{r}} \psi_j(\mathbf{r}) + \sum_{J=A}^D e^{i\mathbf{p}_J\mathbf{r}} \chi_J(\mathbf{r}), \quad (6)$$

where \mathbf{p}_j and \mathbf{p}_J denote the positions of hotspots j and antinodes J , respectively, in the Brillouin zone. The fields for hotspot quasiparticles ψ_j and for antinodal ones χ_J fluctuate only slowly in space on scales much larger than the lattice constant a .

Following Ref. 27, we introduce three pseudospin sec-

tors $L \otimes \Lambda \otimes \Sigma$ to organize the hotspot states,

$$\psi = \left(\left(\left(\begin{array}{c} \psi_1 \\ \psi_2 \\ \psi_3 \\ \psi_4 \end{array} \right)_{\Sigma} \right)_{\Lambda} \right)_L. \quad (7)$$

Inspecting the structure defined in Eq. (7), we see that the sector L organizes the hotspots in the two quartets along the diagonals of the Brillouin zone, cf. Fig. 1(a). Sector Λ distinguishes inside each of the quartets the two pairs of hotspots connected by the antiferromagnetic ordering wave vector \mathbf{Q} . Finally, the pseudospin Σ corresponds to the two hotspots within each of such pairs. The antinodal fields are similarly combined into

$$\chi = \left(\left(\left(\begin{array}{c} \chi_A \\ \chi_B \\ \chi_C \\ \chi_D \end{array} \right)_{\Upsilon} \right)_{\Xi} \right), \quad (8)$$

where Ξ and Υ are two more pseudospins for the four antinodes in Fig. 1(b). Operators acting on these various pseudospin spaces are conveniently expanded in Pauli matrices denoted by, e.g., Υ_1 for the first Pauli matrix in Υ space. Each of the field components ψ_j and χ_J in Eqs. (7) and (8) is itself a spinor for the physical spin, for which we use as usual the Pauli matrix notation $\boldsymbol{\sigma} = (\sigma_1, \sigma_2, \sigma_3)$.

In the approximation of linearized Fermi surfaces close to hotspots and antinodes, the non-interacting part \mathcal{L}_0 of the Lagrangian reads

$$\mathcal{L}_0 = \chi^\dagger (\partial_\tau - i\hat{\mathbf{v}}\nabla) \chi + \psi^\dagger (\partial_\tau - i\hat{\mathbf{V}}\nabla) \psi, \quad (9)$$

where the velocity operator for the antinodal states reads

$$\hat{\mathbf{v}} = -\frac{v}{2} [\Upsilon_3(1 + \Xi_3)\mathbf{e}_x + \Upsilon_3(1 - \Xi_3)\mathbf{e}_y]. \quad (10)$$

Herein, \mathbf{e}_x and \mathbf{e}_y are unit vectors in the directions of Cu bonds and v is the (antinodal) Fermi velocity. The hotspot velocity operator $\hat{\mathbf{V}}$ is a little more complicated. Since we do not use this operator in the present study directly, we refer the reader to Ref. 27.

During the analysis, it will be convenient to study charge and superconducting correlations on equal footing. Therefore, we introduce another pseudospin τ distinguishing particle and hole states,

$$\Psi = \frac{1}{\sqrt{2}} \begin{pmatrix} \psi \\ i\sigma_2\psi^* \end{pmatrix}_\tau, \quad X = \frac{1}{\sqrt{2}} \begin{pmatrix} \chi \\ i\sigma_2\chi^* \end{pmatrix}_\tau. \quad (11)$$

The matrix $C = -\tau_2\sigma_2$ allows for a definition of charge-conjugation

$$\bar{\Psi} = \Psi^t C, \quad \bar{X} = X^t C. \quad (12)$$

In particle-hole space notation, the Lagrangian (9) becomes

$$\mathcal{L}_0 = -\bar{X}(\partial_\tau - i\hat{v}\nabla)X - \bar{\Psi}(\partial_\tau - i\hat{V}\nabla)\Psi, \quad (13)$$

which concludes the non-interacting part of the effective theory.

In order to incorporate the interaction mediated by paramagnons ϕ into the model, we again single out the relevant modes. These are those harmonics of the field ϕ with wave vector close to \mathbf{Q} for hotspot-hotspot interaction and wave vectors at $\mathbf{K}_1, \dots, \mathbf{K}_4$ for hotspot-antinode interactions, see Fig. 1(b). We assume that $\mathbf{K}_1 - \mathbf{K}_2$ is not an inverse lattice vector, which for a general curved Fermi surface is the correct assumption.

In the compact notation, the Lagrangian for interaction at wave vectors $\sim \mathbf{Q}$ is written as²⁷

$$\mathcal{L}_{\text{int},\mathbf{Q}} = \lambda \bar{\Psi}\Sigma_1(\phi_0\sigma)\Psi. \quad (14)$$

Here λ is the coupling constant for the paramagnon-fermion interaction. The general correlation function for ϕ , Eq. (1), translates to the correlation

$$\langle \phi_{0,\omega,\mathbf{q}}^\alpha \phi_{0,-\omega,-\mathbf{q}}^\beta \rangle = \frac{\delta_{\alpha\beta}}{c^{-2}\omega^2 + \mathbf{q}^2 + \xi_{\text{AF}}^{-2}} \quad (15)$$

for the field ϕ_0 entering Eq. (14).

For the interaction at wave vectors $\mathbf{K}_1, \dots, \mathbf{K}_4$, we introduce fields $\phi_{\pm k}$ that are related to field ϕ of Eq. (1) as

$$\phi_{\pm k,\mathbf{q},\omega} = \phi_{\pm\mathbf{K}_k+\mathbf{q},\omega} \quad (16)$$

with correlations

$$\langle \phi_{k,\omega,\mathbf{q}}^\alpha \phi_{-k,-\omega,-\mathbf{q}}^\beta \rangle \simeq \frac{\delta_{\alpha\beta}}{(\Delta K)^2 + \xi_{\text{AF}}^{-2}}. \quad (17)$$

While hotspot-hotspot paramagnons ϕ_0 become critical at the antiferromagnetic QCP ($\xi_{\text{AF}} \rightarrow \infty$), paramagnons $\phi_{\pm k}$ are effectively static as $\Delta K = |\mathbf{K}_1 - \mathbf{Q}| \gg |\mathbf{q}|, c^{-1}\omega$ at low energies. The corresponding Lagrangian reads

$$\mathcal{L}_{\text{int},\mathbf{K}} = 2\lambda \sum_{k=1}^4 \left(\bar{\Psi}T_k(\phi_k\sigma)X + \bar{X}T_k^t(\phi_k\sigma)\Psi \right), \quad (18)$$

where matrices T_k describe the various scattering processes between hotspots and antinodes. They are given by

$$\begin{aligned} T_1 &= \begin{pmatrix} t_3^{\text{B}} & 0 \\ 0 & t_1^{\text{A}} \end{pmatrix}_\tau, & T_2 &= \begin{pmatrix} t_6^{\text{A}} & 0 \\ 0 & t_8^{\text{B}} \end{pmatrix}_\tau, \\ T_3 &= \begin{pmatrix} t_7^{\text{D}} & 0 \\ 0 & t_5^{\text{C}} \end{pmatrix}_\tau, & T_4 &= \begin{pmatrix} t_4^{\text{C}} & 0 \\ 0 & t_2^{\text{D}} \end{pmatrix}_\tau, \end{aligned} \quad (19)$$

where the 8×4 matrices t_j^I are defined by $\psi^\dagger t_j^I \chi = \psi_j^\dagger \chi_j$. While non-trivial effects due to the hotspot Lagrangian $\mathcal{L}_{\text{int},\mathbf{Q}}$, Eq. (14), have been extensively studied in Refs. 26 and 27, we are now in a position to extend the physical picture by effects emerging in the antinodal region, which couple nontrivially to the hotspots via Lagrangian $\mathcal{L}_{\text{int},\mathbf{K}}$, Eq. (18).

B. Emerging orders

1. Pseudogap state

Coupling between hotspot fermions and quantum-critical paramagnons ϕ_0 , Eq. (15), has been studied for a long time. In Ref. 27, it was shown that close to the QCP ($\xi_{\text{AF}} \rightarrow \infty$) below a temperature $T^* \sim \Gamma \sim \lambda^2$, an unusual order parameter composed of two competing suborders appears. These are superconductivity with complex amplitudes Δ_{SC}^1 and Δ_{SC}^2 and a charge order of a spatially modulated quadrupole moment (quadrupole density wave, QDW) with amplitudes Δ_{QDW}^1 and Δ_{QDW}^2 , cf. Eq. (2). Upper indices refer to the two decoupled quartets of hotspots given by $L = 1$ and $L = 2$ states, respectively, cf. Fig. 1(a). This order, hereafter referred to as ‘‘pseudogap’’, constitutes a stable saddle-point manifold in the theory $\mathcal{L}_0 + \mathcal{L}_{\text{int},\mathbf{Q}}$. We incorporate it in terms of a mean-field term that replaces $\mathcal{L}_{\text{int},\mathbf{Q}}$, Eq. (14), in the model. This term is given by

$$\mathcal{L}_{\text{PG}} = \bar{\Psi} b(i\partial_\tau) \mathcal{O}_{\text{PG}} \Psi, \quad (20)$$

where $b(\varepsilon)$ is a function of fermionic Matsubara frequencies ε and \mathcal{O}_{PG} is a matrix in the pseudospin spaces that reflects the symmetry of the order parameter. It reads²⁷

$$\mathcal{O}_{\text{PG}} = i\Sigma_3 \left(\begin{pmatrix} 0 & u_1 \\ -u_1^\dagger & 0 \end{pmatrix}_\Lambda \quad \begin{matrix} 0 \\ \begin{pmatrix} 0 & u_2 \\ -u_2^\dagger & 0 \end{pmatrix}_\Lambda \end{matrix} \right)_L. \quad (21)$$

Here, u_1 and u_2 are $\text{SU}(2)$ matrices in particle-hole space for each of the two quartets of hotspots.

Let us expand the u_j in particle-hole space Pauli matrices τ_i ,

$$u_j = \Delta_0^j + i(\Delta_1^j \tau_1 + \Delta_2^j \tau_2 + \Delta_3^j \tau_3), \quad (22)$$

so that $\Delta_{\text{QDW}}^j = \Delta_0^j + i\Delta_3^j$ and $\Delta_{\text{SC}}^j = \Delta_1^j + i\Delta_2^j$. Numbers Δ_n^j are real and satisfy the constraint $\sum_{n=0}^3 |\Delta_n^j|^2 = 1$ imposed by unitarity. At low energies, we may approximate²⁷ the function $b(\varepsilon)$ as a (positive) constant, $b(\varepsilon) \simeq b_0$.

Study of fluctuations²⁷ of the pseudogap $b(\varepsilon)\mathcal{O}$ shows that below a temperature $T_c < T^*$, one of the suborders—QDW or superconductivity—is suppressed, provided symmetry-breaking effects such as curvature of the Fermi surface are included in the consideration. In the absence of the magnetic field, finite curvature makes the composite order parameter prefer superconductivity as the ground state, whereas a sufficiently strong magnetic field can make a charge modulated state (QDW) energetically more favourable.³⁰ Between T_c and T^* , neither are capable of forming a long-range order and the system is in a regime of strong thermal fluctuations between the two suborders.

2. Antinodal superconductivity

Averaging the Lagrangian (18) over the paramagnon fluctuations ϕ_k , Eq. (17), yields an effective 4-point interaction vertex

$$\mathcal{L}_{\text{int}} = -\frac{4\lambda^2}{(\Delta K)^2} \sum_{k=1}^4 \bar{X} \tau_1 T_k^t \tau_1 \sigma \Psi \bar{\Psi} \sigma \tau_1 T_k \tau_1 X. \quad (23)$$

The model $\mathcal{L}_0 + \mathcal{L}_{\text{PG}} + \mathcal{L}_{\text{int}}$, Eqs. (13), (20), and (23), is the effective model our subsequent study on the physics at the antinodes is based on.

In a mean-field scheme to decouple the interaction \mathcal{L}_{int} , Eq. (23), we replace the $\Psi \bar{\Psi}$ operator by its mean-field correlation function, which by Eqs (13) and (20) is given by

$$\langle \Psi \bar{\Psi} \rangle_{\text{m.f.}} = \frac{J(T)}{4\pi} \mathcal{O}. \quad (24)$$

The function $J(T)$ is defined as

$$J(T) = \frac{\Omega T}{v} \sum_{\varepsilon} \frac{b(\varepsilon)}{\sqrt{\varepsilon^2 + b^2(\varepsilon)}} \quad (25)$$

and $\Omega \sim \lambda^2/v$ is the volume of the hotspot, cf. Ref. 27. Inside the pseudogap regime, the function $J(T) \sim \lambda^4/v^2$ is in a good approximation independent of the temperature T , while it turns to zero when T approaches T^* .

Inserting Eq. (24) into Eq. (23) yields $\mathcal{L}_{\text{int}} \simeq \mathcal{L}_{\text{m.f.}}$ with the mean-field Lagrangian given by

$$\mathcal{L}_{\text{m.f.}} = \frac{3\lambda^2 J(T)}{\pi(\Delta K)^2} [\bar{X} \Xi_3 \Upsilon_1 \{ \Delta_1 \tau_1 + \Delta_2 \tau_2 \} X]. \quad (26)$$

Herein, $\Delta_1 = (\Delta_1^+ - \Delta_1^-)/2$ and $\Delta_2 = (\Delta_2^+ - \Delta_2^-)/2$ form the effective amplitude $\Delta_{\text{SC}} = \Delta_1 + i\Delta_2$ of the hotspot superconductivity. Importantly, in this mean-field treatment, only the superconducting suborder of the hotspot pseudogap gives a contribution, while the QDW does not effectively couple to the fields \bar{X} and X so that it does not play a direct role at the antinodes. Equation (26) thus demonstrates that the hotspot superconductivity induces a superconducting order parameter at the antinodes by the same mechanism sketched in Fig. 1(c) and discussed in Sec. II. The presence of Ξ_3 reflects the d -wave symmetry of the superconducting order. The order parameter of antinodal superconductivity is maximal if

$$\Delta_{1,2}^1 = -\Delta_{1,2}^2, \quad (27)$$

which should be energetically the favoured configuration. Note that the matching condition (27) reduces the $O(4) \times O(4)$ symmetry of the hotspot order to a constrained $O(6)$ model, cf. Ref. 31.

Let us estimate the strength of the superconducting gap induced at the antinodes. According to Eq. (25), we estimate $J(T)$ inside the pseudogap as $J(T) \sim \lambda^4/v^2$, which is smaller than the high energy scale given by the

momentum distance ΔK between hotspots and antinodes. Thus, while the hotspot pseudogap is of order $\Gamma \sim \lambda^2$, the induced antinodal superconducting gap is of order $\lambda^2[\lambda^4/(v\Delta K)^2] \sim \alpha\Gamma \ll \Gamma$, cf. Eq. (3). We emphasize once more that the antinodal superconductivity is induced only if the hotspot system is in the superconducting state.

3. Antinodal charge-density wave order

Let us now address the case when hotspot superconductivity is destroyed by either thermal fluctuations above T_c (pseudogap state) or by a strong enough magnetic field at arbitrary temperature. In the latter case, we obtain QDW at $T < T_c$ or the pseudogap state at $T > T_c$ instead of the superconductor. Then, the mean-field decoupling in Eq. (26) does not induce a finite gap at the antinodes as $\Delta_1 = \Delta_2 = 0$. However, superconducting fluctuations are still present even if $\langle \Delta_1(\mathbf{r}, \tau) \rangle = \langle \Delta_2(\mathbf{r}, \tau) \rangle = 0$. These fluctuations have been studied with the help of a non-linear σ -model in Ref. 27.

At not too high temperatures above the superconducting critical temperature T_c at zero field or below T_c in a sufficiently strong magnetic field destroying the superconductivity, the superconducting fluctuations $\Delta_{\text{SC}}(\mathbf{r}, \tau)$ are small and the σ -model yields the effective Lagrangian

$$\mathcal{L}_{\text{fluct}} \simeq \frac{g\lambda^2}{2} (|\partial_\mu \Delta_{\text{SC}}|^2 + \xi_{\text{SC}}^{-2} |\Delta_{\text{SC}}|^2) \quad (28)$$

with $\partial_\mu = (u^{-1}\partial_\tau, \nabla)$, $g \sim 1$ a coupling constant, and $u \sim v$ the velocity of the fluctuation modes. For $T > T_c$ it is not easy to carry out explicit calculations in the pseudogap state. However, it is well-known³³ that there is no phase transition in the two-dimensional fully isotropic $O(4)$ -symmetric σ -model as all excitations have a gap. In our situation this means that correlation functions of superconducting fluctuations can still formally be obtained from Eq. (28) but the constants entering this equations have now to be considered as effective parameters whose values can hardly be calculated analytically. In the subsequent analysis, we assume that the length ξ_{SC} diverges on the critical line separating the superconducting region from QDW or pseudogap phase.

In the Gaussian approximation of Eq. (28), we immediately integrate the fluctuation modes out of the Lagrangian (26) (, where $\Delta_{\text{SC}} = \Delta_1 + i\Delta_2$ is now assumed to fluctuate both in space and time). Then, we obtain the effective interaction between the antinodal fermions,

$$\begin{aligned} \mathcal{L}_{\text{int,fluct}} = & -\frac{9\lambda^2 J^2(T)}{\pi^2 g(\Delta K)^4} \sum_{j=1}^2 (\bar{X}(\mathbf{r}, \tau) \Xi_3 \Upsilon_1 \tau_j X(\mathbf{r}, \tau)) \\ & \times \Phi(\mathbf{r} - \mathbf{r}', \tau - \tau') (\bar{X}(\mathbf{r}', \tau') \Xi_3 \Upsilon_1 \tau_j X(\mathbf{r}', \tau')), \end{aligned} \quad (29)$$

where

$$\Phi_{\mathbf{q},\omega} = \frac{1}{u^{-2}\omega^2 + \mathbf{q}^2 + \xi_{\text{SC}}^{-2}} \quad (30)$$

is the propagator of superconducting fluctuations. At the transition, $\xi_{SC} \rightarrow \infty$ and this propagator is singular in the infrared limit, which makes the antinodal points effectively hot. Moreover, opposite antinodes are effectively nested. We emphasize, though, that, in analogy with the hotspot fermions interacting via critical paramagnons, this effective nesting is due to the singular form of the propagator of superconducting fluctuations in the vicinity of the superconductor transition where the length ξ_{SC} diverges. This does not necessarily require a geometrically flat Fermi surface at the antinodes.

The interaction (29) generates an instability toward

charge-density wave (CDW) order. Indeed, the Lagrangian (29) for the interaction of antinodal fermions has effectively the same form as the effective interaction induced by paramagnons that is responsible for the formation of the pseudogap. We thus introduce a CDW order parameter in the Lagrangian,

$$\mathcal{L}_{CDW} = \bar{X} b_{CDW} (i\partial_\tau) \mathcal{O}_{CDW} X, \quad (31)$$

and obtain in analogy with Ref. 27 the mean-field equation

$$b_{CDW}(\varepsilon) \mathcal{O}_{CDW} = -\frac{9\lambda^2 J^2(T)}{\pi^2 g(\Delta K)^4} \sum_{j=1}^2 T \sum_{\varepsilon', \mathbf{k}'} \Phi_{\mathbf{k}', \varepsilon - \varepsilon'} \Xi_3 \Upsilon_1 \tau_j \frac{b_{CDW}(\varepsilon') \mathcal{O}_{CDW}}{\varepsilon'^2 + (v\mathbf{k}')^2 + b_{CDW}^2(\varepsilon')} \Xi_3 \Upsilon_1 \tau_j. \quad (32)$$

Deriving Eq. (32) has required that \mathcal{O}_{CDW} anticommutes with the velocity operator \hat{v} , Eq. (10), which implies $\{\mathcal{O}_{CDW}, \Upsilon_3\} = 0$ and $[\mathcal{O}_{CDW}, \Xi_3] = 0$. In addition, we assume the normalization $\mathcal{O}_{CDW}^2 = 1$. Furthermore, in order to compensate for the minus sign in Eq. (32), we need to impose that $\{\mathcal{O}_{CDW}, \Upsilon_1 \tau_1\} = 0$ and $\{\mathcal{O}_{CDW}, \Upsilon_1 \tau_2\} = 0$. Summarizing all these constraints, the antinodal order parameter becomes

$$\mathcal{O}_{CDW} = \begin{pmatrix} \Delta'_x \Upsilon_1 \tau_3 + \Delta''_x \Upsilon_2 & 0 \\ 0 & \Delta'_y \Upsilon_1 \tau_3 + \Delta''_y \Upsilon_2 \end{pmatrix} \Xi. \quad (33)$$

Parameters Δ'_x and Δ''_x play the roles of real and imaginary parts for the order parameter of CDW in x -direction while Δ'_y and Δ''_y do so for the y -direction. They satisfy the nonlinear constraints $[\Delta'_x]^2 + [\Delta''_x]^2 = 1$ and $[\Delta'_y]^2 + [\Delta''_y]^2 = 1$.

Measuring all quantities of dimension of energy in units of

$$\Gamma_{CDW} = \frac{18u\lambda^2 J^2}{\pi^2 g v (\Delta K)^4}, \quad (34)$$

we derive from Eq. (32) a *universal* self-consistency equation for the CDW amplitude $b_{CDW}(\varepsilon)$,

$$\bar{b}_{CDW}(\varepsilon) = \bar{T} \sum_{\varepsilon'} \frac{1}{|\varepsilon - \varepsilon'|} \frac{\bar{b}_{CDW}(\varepsilon')}{\sqrt{\varepsilon'^2 + b_{CDW}^2(\varepsilon')}}. \quad (35)$$

In this equation, all quantities z of dimension energy enter in the form $\bar{z} = z/\Gamma_{CDW}$. The energy scale $\Gamma_{CDW} \sim \alpha^2 \Gamma$, cf. Eq. (3), is smaller than both the pseudogap energy scale $\sim \Gamma$ and the antinodal superconducting gap $\sim \alpha \Gamma$, which appears when the pseudogap has ordered into the superconducting suborder. Numerical investigation of Eq. (35) indicates non-zero solutions

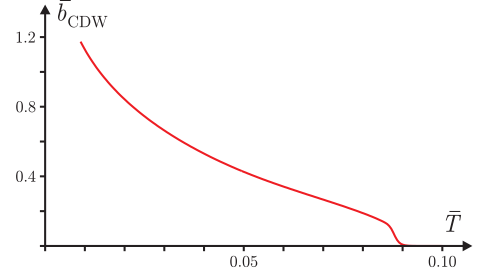


FIG. 3. Dimensionless charge-density gap $\bar{b}_{CDW} = b_{CDW}/\Gamma_{CDW}$ as a function of dimensionless temperature \bar{T} interpolated to the frequency $\varepsilon = 0$. A CDW order appears below the temperature $T_{CDW} \approx 0.09\Gamma_{CDW}$.

for $b_{CDW}(T, \varepsilon)$ below a temperature $T_{CDW} \approx 0.09\Gamma_{CDW}$. Figure 3 shows the (interpolated) amplitude $b_{CDW}(T, 0)$ as a function of temperature T .

Calculating the charge density in the presence of the order parameter \mathcal{O}_{CDW} , Eq. (33), we obtain formula (5) for the bidirectional CDW modulation,

$$\rho_{CDW}(\mathbf{r}) \sim \frac{e\Gamma_{CDW}^2}{v^2} \{ \cos(\mathbf{Q}_x \mathbf{r} + \varphi_x) + \cos(\mathbf{Q}_y \mathbf{r} + \varphi_y) \}, \quad (36)$$

where φ_x and φ_y denote the phases of the CDW order in x and y directions, respectively. Thus, the charge density is modulated with the wave vectors \mathbf{Q}_x and \mathbf{Q}_y connecting two opposite antinodal points. This contrasts the modulations of the quadrupole-density D_{xx} generated²⁷ at the hotspots in the presence of QDW,

$$D_{xx}(\mathbf{r}) \sim e \{ |\Delta_{QDW}^1| \cos(\mathbf{Q}_1 \mathbf{r} + \varphi_1) + |\Delta_{QDW}^2| \cos(\mathbf{Q}_2 \mathbf{r} + \varphi_2) \}. \quad (37)$$

QDW wave vectors \mathbf{Q}_1 and \mathbf{Q}_2 are turned by 45° and longer than the CDW wave vectors by a factor roughly

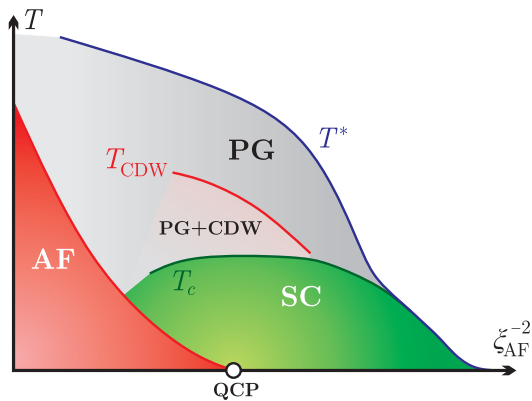


FIG. 4. Qualitative phase diagram summarizing the results of Ref. 27 and the present work for zero magnetic field. Close to the antiferromagnetic (AF) QCP, $\xi_{\text{AF}}^{-2} = 0$, and upon lowering the temperature, the system develops first at T^* the instability toward the fluctuating pseudogap state (PG) characterized by the order parameter of Eq. (2). At lower temperatures $T < T_{\text{CDW}} < T^*$, strong superconducting fluctuations induce a transition toward charge density wave (CDW) formed at the antinodes. Finally, below T_c , the particle-hole suborder of the pseudogap prevails due to curvature effects and establishes d -wave superconductivity.

given by $\sqrt{2}$. Both orders form checkerboards as illustrated in Fig. 2. Figure 2(c) shows the type of particle-hole order, i.e. whether QDW or CDW, as a qualitative function of the position on the Fermi surface. Whereas within our model hotspot and antinodal regions are separated, we expect in realistic systems regions of small overlap of the two orders in between.

IV. CUPRATE PHYSICS

We now address the phase diagram of cuprates in the proximity of the antiferromagnetic QCP. We emphasize that our theory applies only to the “metallic” side of the antiferromagnet–normal metal phase transition. The regions of too low doping are thus excluded in the following discussion. In the region of intermediate doping, suppression of carrier density below a crossover temperature T^* observed in NMR measurements^{34,35} was the first evidence for the existence of a “pseudogap” in the electron spectrum. In contrast, d -wave superconductivity appears only below a considerably lower temperature T_c . In our theory, T^* is associated with the crossover to the strongly fluctuating $O(4)$ -symmetric composite order (superconductivity and QDW) close to the hotspots.²⁷ The phase diagram, see Fig. 4, is further enriched by the formation of CDW order with wave vectors $\mathbf{Q}_{x,y}$ (Fig. 2) at the edge of the Brillouin zone. Also the emergence of the CDW order is ultimately due to the proximity to the QCP. The additional phase transition is expected to occur at a temperature T_{CDW} inside the pseudogap phase, $T_c < T_{\text{CDW}} < T^*$.

The charge modulation observed in various recent experiments^{4–12} has been attributed^{27,29} to the existence of QDW (or “bond order”) correlations. This picture is, in principle, in agreement with NMR results⁷ and sound propagation measurements^{11,36}. However, STM studies^{4–6} of BSCCO and experiments with hard^{9,12} and resonant soft^{8,10} X-ray scattering on YBCO have revealed a charge modulation along the bonds of the Cu lattice with modulation vectors close to $\mathbf{Q}_{x,y}$, which are the CDW wave vectors. Moreover, QDW has a vanishing Fourier transform near even Bragg peaks. Therefore, STM and hard X-ray experiments can hardly be expected to detect the QDW modulation.

The seeming contradiction is resolved when we include the CDW, Eq. (5), in the Cu lattice. Then, this explains the experimental results^{4–12}. CDW appears below a critical temperature T_{CDW} that can be considerably lower than T^* , in line with the results of the hard X-ray experiment of Ref. 9. In addition, Hall effect measurements³⁷ indicate a reconstruction of the Fermi surface that is attributed to the formation of CDW. The transition temperatures T_{CDW} of these two experiments agree with each other. Evidence for a transition below T^* and related to CDW has also been found recently in a Raman scattering study.³⁸ The dual effect of the two modulations (QDW and CDW) on the two species of atoms in the CuO plane is a characteristic of our theory and might be tested via resonant soft X-ray scattering.

Very recent STM and resonant elastic X-ray experiments^{39,40} on BSCCO confirm the CDW wave vectors’ orientation along the bonds but indicate that they connect hotspots rather than antinodes. In our model, we expect CDW to set in at wave vectors as soon as the QDW gap is small. In realistic systems, this may indeed happen already not very far from the hotspots, possibly enhanced by reconstruction of the Fermi surface. Details behind this physics are clearly beyond the range of our “minimal model” and left for a separate study.

The emergence of various gaps in \mathbf{k} -space around the Fermi surface has been reported in Raman scattering on Bi-2212 and Hg-1201 compounds.⁴¹ It was demonstrated that in overdoped samples the superconducting gap spreads all over the Fermi surface. In contrast, in underdoped samples the coherent Cooper pairs are observed mostly near the nodes, whereas the gap at the antinodes is mainly of a non-superconducting origin. This effect can naturally be explained within our picture because the hotspots move to nodes with decreasing the doping and the superconducting gap at the antinodes should decrease. At the same time, the CDW gap grows at the antinodes thus “pushing away” the Cooper pairs.

We note that after our work has been completed and distributed as a preprint on arXiv, a work discussing the issue of the rotation of the charge order wave vector by 45° has appeared.⁴² A solution of mean-field equations for a new CDW suggested in the latter work, although very interesting, is not stable against formation

of SC/QDW order of Ref. 27 below its transition temperature T^* . As a result, new preemptive states predicted in Ref. 42 may be possible only in the vicinity of T^* .

V. CONCLUSION

Extending the analysis of the spin-fermion model for the two-dimensional antiferromagnetic QCP to the antinodal regions, we find below the pseudogap temperature T^* another transition to a bidirectional CDW induced at the zone edge by superconducting fluctuations. The physics behind this transition is determined by pseudogap physics emerging at the hotspots. Our theory thus

shows how a complexity of offspring phases arises out of the single QCP. The results enable us to address recently observed charge order features in the phase diagram of the high- T_c cuprates.

ACKNOWLEDGMENTS

K.B.E. acknowledges support by the Chaire Blaise Pascal award of the Région Île-de-France. H.M. acknowledges the Yale Prize Postdoctoral Fellowship. Financial support (K.B.E., H.M., and M.E.) by SFB/TR12 of DFG is gratefully appreciated.

-
- ¹ J. G. Bednorz, K. A. Müller, *Z. Physik* **64B**, 189 (1986).
² P. A. Lee, N. Nagaosa, X. G. Wen, *Rev. Mod. Phys.* **78**, 17 (2006).
³ M. R. Norman, C. Pépin, *Rep. Prog. Phys.* **66**, 1547 (2003).
⁴ W. D. Wise, M. C. Boyer, K. Chatterjee, T. Kondo, T. Takeuchi, H. Ikuta, Y. Wang, and E. W. Hudson, *Nat. Phys.* **4**, 696 (2008).
⁵ M. J. Lawler, K. Fujita, J. Lee, A. R. Schmidt, Y. Kohsaka, C. K. Kim, H. Eisaki, S. Uchida, J. C. Davis, J. P. Sethna, and E.-A. Kim, *Nature* **466**, 347 (2010).
⁶ C. V. Parker, P. Aynajian, E. H. da Silva Neto, A. Pushp, S. Ono, J. Wen, Z. Xu, G. Gu, and A. Yazdani, *Nature* **468**, 677 (2010).
⁷ T. Wu, H. Mayaffre, S. Krämer, M. Horvatić, C. Berthier, W. N. Hardy, Ruixing Liang, D. A. Bonn, and M.-H. Julien, *Nature* **477**, 191 (2011).
⁸ G. Ghiringhelli, M. Le Tacon, M. Minola, S. Blanco-Canosa, C. Mazzoli, N. B. Brookes, G. M. De Luca, A. Frano, D. G. Hawthorn, F. He, T. Loew, M. Moretti Sala, D. C. Peets, M. Salluzzo, E. Schierle, R. Sutarto, G. A. Sawatzky, E. Weschke, B. Keimer, and L. Braicovich, *Science* **337**, 821 (2012).
⁹ J. Chang, E. Blackburn, A. T. Holmes, N. B. Christensen, J. Larsen, J. Mesot, Ruixing Liang, D. A. Bonn, W. N. Hardy, A. Watenphul, M. v. Zimmermann, E. M. Forgan, and S. M. Hayden, *Nat. Phys.* **8**, 871 (2012).
¹⁰ A. J. Achkar, R. Sutarto, X. Mao, F. He, A. Frano, S. Blanco-Canosa, M. Le Tacon, G. Ghiringhelli, L. Braicovich, M. Minola, M. Moretti Sala, C. Mazzoli, Ruixing Liang, D. A. Bonn, W. N. Hardy, B. Keimer, G. A. Sawatzky, and D. G. Hawthorn, *Phys. Rev. Lett.* **109**, 167001 (2012).
¹¹ D. LeBoeuf, S. Krämer, W. N. Hardy, Ruixing Liang, D. A. Bonn, and C. Proust, *Nat. Phys.* **9**, 79 (2013).
¹² E. Blackburn, J. Chang, M. Hücker, A. T. Holmes, N. B. Christensen, Ruixing Liang, D. A. Bonn, W. N. Hardy, U. Rütt, O. Gutowski, M. v. Zimmermann, E. M. Forgan, and S. M. Hayden, *Phys. Rev. Lett.* **110**, 137004 (2013).
¹³ J. Zaanen and O. Gunnarsson, *Phys. Rev. B* **40**, 7391(R) (1989).
¹⁴ K. Machida, *Physica C* **158**, 192 (1989).
¹⁵ J. M. Tranquada, B. J. Sternlieb, J. D. Axe, Y. Nakamura, S. Uchida, *Nature* **375**, 561-563 (1995).
¹⁶ V. J. Emery, S. A. Kivelson, J. M. Tranquada, *Proc. Natl. Acad. Sci. USA* **96**, 8814 (1999).
¹⁷ S. A. Kivelson, I. P. Bindloss, E. Fradkin, V. Oganesyan, J. M. Tranquada, A. Kapitulnik, and C. Howald, *Rev. Mod. Phys.* **75**, 1201 (2003).
¹⁸ S. Chakravarty, R. B. Laughlin, D. K. Morr, C. Nayak, *Phys. Rev. B* **63**, 094503 (2001).
¹⁹ S. Sachdev, *Quantum Phase Transitions*, Cambridge University Press, New York (1998).
²⁰ S. Sachdev and B. Keimer, *Physics Today* **64**, 29 (2011).
²¹ A. J. Millis and H. Monien, *Phys. Rev. Lett.* **70**, 2810 (1993).
²² H. Loney, A. Rosch, M. Vojta, and P. Wölfle, *Rev. Mod. Phys.* **79**, 1015 (2007).
²³ A. W. Rost, S. A. Grigera, J. A. N. Bruin, R. S. Perry, D. Tian, S. Raghu, S. A. Kivelson, and A. P. Mackenzie, *Proc. Natl. Acad. Sci. USA* **108**, 16549 (2011).
²⁴ Ar. Abanov, A. V. Chubukov, *Phys. Rev. Lett.* **84**, 5608 (2000).
²⁵ Ar. Abanov, A. V. Chubukov, J. Schmalian, *Adv. Phys.* **52**, 119 (2003).
²⁶ M. A. Metlitski and S. Sachdev, *Phys. Rev. B* **82**, 075128, (2010).
²⁷ K. B. Efetov, H. Meier, and C. Pépin, *Nat. Phys.* **9**, 442 (2013).
²⁸ J. A. Hertz, *Phys. Rev. B* **14**, 1165 (1976).
²⁹ S. Sachdev, R. La Placa, *Phys. Rev. Lett.* **111**, 027202 (2013).
³⁰ H. Meier, M. Eichenkel, C. Pépin, K. B. Efetov, *Phys. Rev. B* **88**, 020506(R) (2013).
³¹ L. E. Hayward, D. G. Hawthorn, R. G. Melko, S. Sachdev, *Science* **343**, 1336 (2014).
³² Ar. Abanov, A. V. Chubukov, M. R. Norman, *Phys. Rev. B* **78**, 220507(R) (2008).
³³ J. Zinn-Justin, *Quantum Field Theory and Critical Phenomena*, Clarendon Press, Oxford (1996).
³⁴ W. W. Warren, R. E. Walstedt, G. F. Brennert, R. J. Cava, R. Tycko, R. F. Bell, and G. Dabbagh, *Phys. Rev. Lett.* **62**, 1193 (1989).
³⁵ H. Alloul, T. Ohno, P. Mendels, *Phys. Rev. Lett.* **63**, 1700 (1989).
³⁶ A. Shekhter, B. J. Ramshaw, Ruixing Liang, W. N. Hardy, D. A. Bonn, F. F. Balakirev, R. D. McDonald, J. B. Betts, S. C. Riggs, and A. Migliori, *Nature* **498**, 75 (2013).

- ³⁷ D. LeBoeuf, N. Doiron-Leyraud, B. Vignolle, M. Sutherland, B. J. Ramshaw, J. Levallois, R. Daou, F. Laliberté, Olivier Cyr-Choinière, J. Chang, Y. J. Jo, L. Balicas, Ruixing Liang, D. A. Bonn, W. N. Hardy, C. Proust, and L. Taillefer, *Phys. Rev. B* **83**, 054506 (2011).
- ³⁸ M. Bakr, S. M. Souliou, S. Blanco-Canosa, I. Zegkinoglou, H. Gretarsson, J. Stempfer, T. Loew, C. T. Lin, R. Liang, D. A. Bonn, W. N. Hardy, B. Keimer, and M. Le Tacon, *Phys. Rev. B* **88**, 214517 (2013).
- ³⁹ R. Comin, A. Frano, M. M. Yee, Y. Yoshida, H. Eisaki, E. Schierle, E. Weschke, R. Sutarto, F. He, A. Soumyanarayanan, Yang He, M. Le Tacon, I. S. Elfimov, J. E. Hoffman, G. A. Sawatzky, B. Keimer, and A. Damascelli, *Science* **343**, 390 (2014).
- ⁴⁰ E. H. da Silva Neto, P. Aynajian, A. Frano, R. Comin, E. Schierle, E. Weschke, A. Gyenis, J. Wen, J. Schneeloch, Z. Xu, S. Ono, G. Gu, M. Le Tacon, A. Yazdani, *Science* **343**, 393 (2014).
- ⁴¹ A. Sacuto, Y. Gallais, M. Cazayous, M.-A. Méasson, G. D. Gu, and D. Colson, *Rep. Prog. Phys.* **76**, 022502 (2013).
- ⁴² Y. Wang, A. V. Chubukov, arXiv:1401.0712 (2014).